Synthesis and Physical Properties of Poly(fluoroalkylether)urethanes

X-H. YU* and A. Z. OKKEMA, *Material Science Program, University of Wisconsin-Madison, Madison, Wisconsin 53706,* and S. L. COOPER,† *Department of Chemical Engineering, University of Wisconsin-Madison, Madison, Wisconsin 53706*

Synopsis

Polyurethane block copolymers were synthesized containing between 33 and 50 wt % hard segments based on 4,4'-diphenylmethane diissocyanate (MDI) and either 1,4-butanediol (BD), or *N*-methyldiethanolamine (MDEA) as the chain extender. The soft segments were composed of poly(tetramethylene oxide) (PTMO) and fluoropolyether glycol (FPEG) oligomers (M_n = 1000 and 1899, respectively), copolymerized to produce polyurethanes containing 5–100 wt % FPEG soft segment. The PTMO polyol in one sample was substituted with a tetrahydrofuran/ethylene oxide polyol (75 : 25 mole ratio) (M_n = 1140). The MDEA-extended polymer was ionized using 1,3-propane sultone. The bulk and surface properties of these polymers were evaluated by a variety of techniques. Differential scanning calorimetry (DSC) and dynamic mechanical analysis showed that the incorporation of 5–14 wt % FPEG into the soft segment had essentially no effect on the polymer's multiphase structure. The ultimate tensile strength and elongation was reduced by the addition of FPEG. Chain extending with BD as opposed to MDEA improved phase separation and the ultimate tensile strength. In vacuum, surface enrichment of the low surface energy FPEG was observed for all the polymers, using X-ray photoelectron spectroscopy (XPS). The dynamic contact angle results indicate that the polymer surfaces rearranged in an aqueous environment to minimize their interfacial free energy.

INTRODUCTION

Thermoplastic polyurethane elastomers are block copolymers consisting of alternating soft and hard segments. The soft segment is in a viscous or rubbery state, providing elastomeric character to the polymer. The hard segment is glassy or semicrystalline and provides dimensional stability to the polymer by acting as a thermally reversible and multifunctional crosslink as well as a reinforcing filler. In the solid state the hard and soft segments of the copolymer aggregate into separate microdomains, which results in an elevated rubbery plateau modulus and generally other enhanced physical properties.

In conventional linear segmented polyurethanes the soft segments are commonly low molecular weight (600–3000) polyether or polyester macroglycols. The hard segments generally consist of an aromatic diisocyanate that is chain extended with a low molecular weight diol to produce blocks with a distribution of molecular weights. The driving force for phase separation in these systems

* Visiting Scholar from Nanjing University, Department of Chemistry, People's Republic of China.

† To whom correspondence should be addressed.

Journal of Applied Polymer Science, Vol. 41, 1777–1795 (1990)
 CCC 0021-8995/90/7-81777-19$04.00

is the incompatibility of the soft and hard segments. The wide range of polymer morphologies and physical properties observed for polyurethane block copolymers, depends upon the composition and chemical structure of the hard and soft segments.[1-3]

Fluorinated polymers are of interest due to their excellent thermal and oxidative stability,[4] low surface tension, low friction,[5,6] good chemical resistance,[7] and their excellent oxygen permeability.[8] The ability of fluoropolymers to dissolve oxygen has led to their use in artificial blood applications.[9] The unique characteristics of fluorinated polymers are in part due to their low surface energy, which results from the migration of the fluorine containing groups to the air–polymer interface providing a very hydrophobic surface.

Until recently, polyurethanes containing fluorinated alkylether soft segments have received little attention.[6] However, fluorinated polyurethanes prepared from conventional polyols but containing fluorinated diisocyanates and fluorinated short-chain diols have been extensively studied.[10-13] Polyurethanes prepared from fluorinated diols generally lack the extensibility of their nonfluorinated analogs,[10,11] while polyurethanes based on perfluoroalkyl diisocyanates are hydrolytically unstable.[12] Preliminary studies of polyurethanes containing fluorinated hydroxyl-terminated polyethers have shown that these polymers are both extensible and hydrolytically stable.[12] It is expected that the inclusion of a low molecular weight, nonpolar, fluoropolyether glycol into a polyurethane should alter the polymer's bulk and surface properties resulting in polyurethanes suitable for a variety of new applications.

In this investigation, a series of eight polyetherurethane block copolymers containing between 33 and 50 wt % hard segments based on 4,4′-diphenylmethane diisocyanate (MDI), 1,4-butanediol (BD), or *N*-methyldiethanolamine (MDEA) were synthesized. Four of the polymers were copolymerized using polytetramethylene oxide (PTMO) (MW = 1000) and fluoropolyether glycol (FPEG) (MW = 1899) to produce polyurethanes containing mixed soft segments having 5–14 wt % FPEG with approximately the same hard segment content (43–48 wt %). The PTMO macroglycol in one of the mixed soft segment polymers was replaced with a tetrahydrofuran ethylene oxide polyol (THF/EO) (75 : 25) (M_n = 1140). The other four polymers contained pure FPEG soft segments with varying percentages of hard segment and two types of chain extender. A zwitterionomer of the MDEA chain-extended polymer was formed by the reaction of propane sultone with the tertiary nitrogen of MDEA.

The composition and sample designation for the polymers studied are described in Table I. An example of the sample code for a mixed macroglycol polymer is B47-F5. B47 represents the 1,4-butanediol chain extender and the weight percentage of hard segment, while the F5 signifies that the soft segment contains 5 wt % FPEG with the remainder being PTMO (MW = 1000). Similarly, M indicates the chain extender is MDEA and S8 indicates the weight percent of propane sultone substituted onto the tertiary nitrogen of the MDEA chain extender.

In this study, the microphase morphology, bulk, and surface properties of these polyurethanes were evaluated to determine what effect variations in the chain architecture such as the addition of FPEG into the PTMO soft segment, the percent hard segment, the type of chain extender, and the incorporation of ionic groups had on these properties.

TABLE I
Material Characterization

Sample code	Composition	Molecular weight[a] ($\overline{M}_n$)
B48-F0	48 wt % MDI/BD 52 wt % PTMO (1000 MW)	41,000
B47-F5	47 wt % MDI/BD 48 wt % PTMO (1000 MW) 4.8 wt % FPEG (1899 MW)	40,000
B46-F9	46 wt % MDI/BD 45 wt % PTMO (1000 MW) 9.4 wt % FPEG (1899 MW)	35,000
B45-F14	45 wt % MDI/BD 41 wt % PTMO (1000 MW) 13.8 wt % FPEG (1899 MW)	42,000
B43-F9-EO8	43 wt % MDI/BD 48 wt % THF/EO polyol 75 : 25 mole ratio (1140 MW) 9.4 wt % FPEG (1899 MW)	32,000
B50-F50	50 wt % MDI/BD 50 wt % FPEG (1899)	40,000
B33-F67	33 wt % MDI/BD 67 wt % FPEG (1899)	38,000
M34-F66	34 wt % MDI/MDEA 66 wt % FPEG (1899)	35,000
M34-F66-S8	PEU–MDEA-34 reacted with 8 wt % propane sultone	—

[a] Based on polystyrene standards.

EXPERIMENTAL METHODS

Synthesis

The fluorinated polyether glycol (FPEG) was kindly provided by Dr. E. Pechhold of E. I. DuPont de Nemours & Co. The FPEG macroglycol had a number average molecular weight of M_n = 1899 and a fluorine content of 48.3 wt %. As shown in Scheme 1, FPEG is composed of a polyether backbone with a short pendant perfluoroalkyl side group.

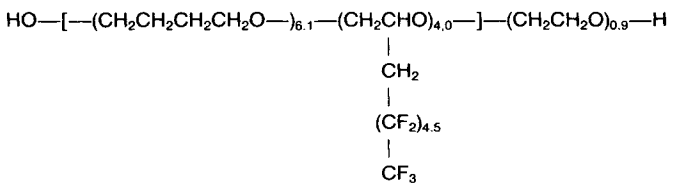

Scheme 1. Structure of fluoropolyether glycol (FPEG).

The macroglycol was purified prior to use by washing it three times with distilled water until pH 7 was attained, and then it was dried under vacuum at 70°C for 24 h. The MDI (Polysciences) was melted and pressure filtered at 60°C. Previous experiments in our laboratory have shown that pressure filtration and vacuum distillation are equivalent methods of purification for MDI. *N,N*-dimethylacetamide (DMAc) (Aldrich) was dehydrated over calcium hydride for 2 days and then vacuum distilled. Tetrahydrofuran (THF) (Aldrich) HPLC grade was kept over molecular sieves, while BD (Aldrich), MDEA (Aldrich), stannous octoate catalyst (M&T Chemicals), and 1,3-propane sultone (Aldrich), a known carcinogen, were used as received.

The segmented poly(fluoroalkylether)urethanes examined in this study were synthesized by a two-step addition reaction. Solutions of FPEG and MDI were prepared in THF and DMAc, respectively. A mixture of solvents, THF and DMAc, was used in the synthesis to avoid macrophase separation of the reactants due to their different solubilities. The FPEG solution, containing 0.15% stannous octoate catalyst was slowly added to the stirred MDI solution at 60–70°C under dry argon. These reactants were miscible throughout the synthesis as indicated by the clarity of the solution. After an hour, the chain extender was added, and stirring was continued at 80–85°C. Chain extension with BD or MDEA required 6 h. After a satisfactory molecular weight had been achieved, as determined by gel permeation chromatograph (GPC) analysis, the polymer was precipitated in hot distilled water, washed with ethyl alcohol, and then dried in a vacuum oven at 70–80°C for a minimum of 2 days. The polymer yield in all cases was greater than 90%. The fluorine-containing polyurethanes were soluble in THF.

Polymers with copolymerized mixed soft segments (FPEG : PTMO) were synthesized by a similar procedure except that the FPEG solution was added first and allowed to react for one hour to avoid phase separation of the reactants. A PTMO/DMAc solution was then added and the reaction was continued for another hour.

Zwitterionization, as shown in Scheme 2, was carried out on a portion of the MDEA-extended polymer by first dissolving it in DMAc. A stoichiometric amount of 1,3-propane sultone was added to the solution, and the reaction mixture was stirred at 40–50°C for 3 h.

Sample Preparation

Films of the polyurethane block copolymers were spin cast from a 10% THF solution, dried in a vacuum oven at 65°C for 2 days, and then stored in a desiccator at room temperature. Film thickness ranged from 100 to 500 μm

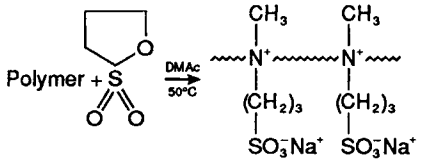

Scheme 2. Synthetic scheme for zwitterionization of the MDI/MDEA/FPEG polymer.

depending upon the requirements of a given experiment. The films were translucent to visible light.

Underwater contact angle evaluation and X-ray photoelectron spectroscopy (XPS) were performed on samples coated onto the inner diameter of oxidized polyethylene (PE) tubing (Intramedic, Clay-Adams, 3.18 mm ID) following the protocol described by Lelah et al.[14] A 10 w/v% THF solution of each polymer was used for the coating procedure.

Bulk Characterization

An estimate of the number average molecular weight of the polymers was obtained using a Waters Associates Model 501 high-pressure GPC using THF as the mobile phase. The apparent number average molecular weights were calculated on the basis of the molecular weight versus retention volume curve of monodisperse polystyrene standards.

Transmission infrared survey spectra were recorded with a Nicolet 7199 Fourier transform infrared spectrophotometer operated with a dry air purge. Two hundred scans at a resolution of 2 cm^{-1} were signal-averaged before Fourier transformation.

Thermal analysis was carried out on a Perkin-Elmer DSC-7 interfaced with a Perkin-Elmer Model 7500 Thermal Analysis Data Station (TADS) computer. The data processing unit allows subtraction of the background and normalization of the thermogram for sample weight. Temperature and enthalpy calibration were carried out using indium and mercury standards. A heating rate of 20 K/min under a N_2 purge was used.

Dynamic mechanical data were obtained using a microprocessor controlled Rheovibron DDV-II. All measurements were carried out under a N_2 purge at a frequency of 110 Hz with a constant heating rate of 3°C/min.

Room temperature uniaxial stress–strain tests were performed using an Instron table model tensile testing device at a crosshead speed of 0.5 in./min. Dumbbell-shaped samples with a gauge length of 0.876 in. were stamped out using an ASTM D-1708 die.

Surface Characterization

XPS spectra were obtained using a Physical Electronics PHI 5400 spectrometer with a 300-W, 15-kV magnesium anode. Widescan spectra were obtained at a pass energy of 89.45 eV. High-resolution spectra were recorded for all elements present, at a pass energy of 35.75 eV. The relative atomic percentage of each element at the surface was estimated from peak areas using atomic sensitivity factors specific for the PHI 5400. These factors account for the Scofield photoelectron cross sections,[15] the kinetic energy dependence of the inelastic mean free path of emitted electrons, and the electron kinetic energy dependence of the transmission function $T(E_k)$.[16]

In order to analyze the chemical bonding of the carbon atoms, a higher resolution spectra of carbon was obtained at a pass energy of 17.90 eV. The high-resolution C_{1s} spectrum for B33-F67, shown in Figure 1, is representative of the other polymer spectra. The C_{1s} high-resolution spectrum was smoothed and then deconvoluted using a van Cittert routine[17] available in the PHI 5400 computer software. The five peaks were curve fit using a combination of Gauss-

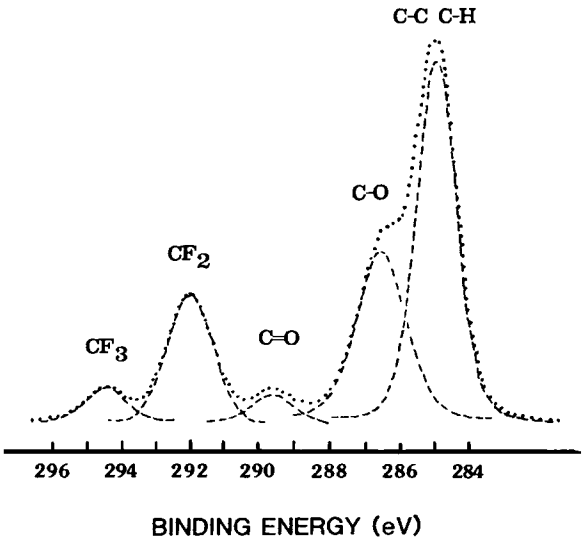

Fig. 1. High resolution C_{1s} spectra of B33-F67.

ian and Lorentzian peak shapes. These peaks correspond to aliphatic and aromatic carbon (C—C, C—H) referenced at 285 eV,[18,19] ether carbon at approximately 286.5 eV, carbonyl carbon (C=O) at approximately 290 eV, carbon bonded to two fluorine atoms (CF_2) at approximately 292.0 eV, and carbon bonded to three fluorine atoms (CF_3) at approximately 294.5 eV.[19,20]

Underwater contact angle measurements were made using the technique of Hamilton,[21] modified for use on curved surfaces.[14] The surfaces were equilibrated with double-distilled, deionized water for 24 h prior to the collection of data. A minimum of 10 measurements were used to calculate the average surface–water–air and surface–water–octane contact angles.

Dynamic contact angle measurements were obtained using a Cahn surface analyzer. Polymer-coated coverslips were immersed and subsequently drawn out of high-purity water at a speed of 21 mm^{-1}. The force versus immersion depth curve was obtained and the advancing and receding angles were calculated from the curves as described by Andrade et al.[22]

RESULTS AND DISCUSSION

Bulk Characterization

The GPC analysis of these polymers was performed to verify that reasonable molecular weights were obtained. The apparent number average molecular weights, based on polystyrene standards, are shown in Table I.

Infrared Spectroscopy

The transmission infrared spectra for B48-F0, B45-F14, and B50-F50 are shown in Figure 2 and are representative of the other samples. The incorporation of FPEG into the polymer backbone was verified[23] by the two C–F absorbance

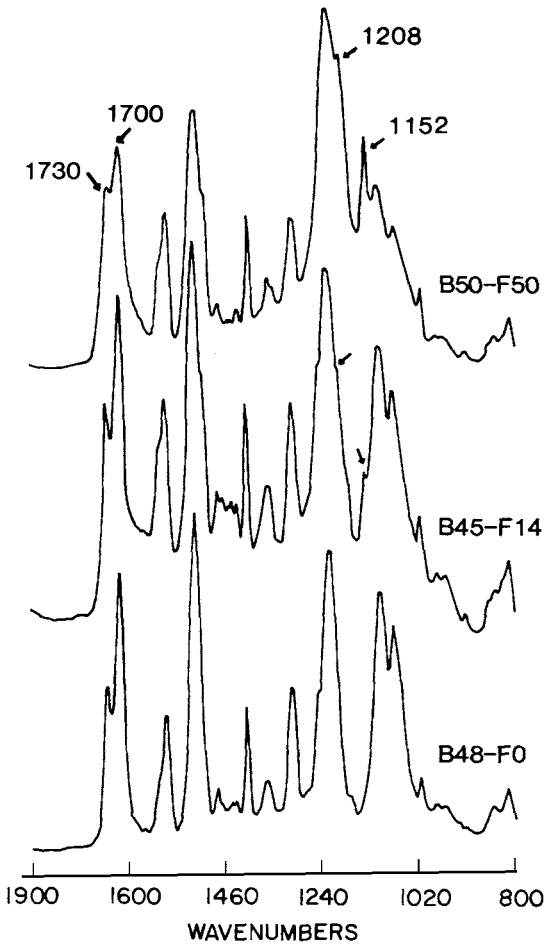

Fig. 2. Transmission IR spectra for B50-F50, B48-F0, and B45-F14.

bands at 1152 and 1208 cm^{-1} shown in Figure 2. As expected, the intensity of the C–F absorbance peaks increased with the wt % FPEG in the polymer backbone. The other absorbance peaks in the IR spectra are representative of a typical polyetherurethane block copolymer.

Nearly all the N–H groups are hydrogen bonded as indicated by the absence of an absorbance peak at 3450 cm^{-1}. In polyetherurethanes hydrogen bonding can occur between the urethane N–H groups and the hard segment carbonyl oxygen and alkoxy oxygen along with the soft segment ether oxygen.[24,25] The ratio of the hydrogen-bonded urethane carbonyl absorbance at 1700 cm^{-1} to the free carbonyl absorbance at 1732 cm^{-1} provide a qualitative estimation of the degree of phase separation in polyurethanes on a microscopic level.[24] An increase in the bonded–free carbonyl ratio indicates an increase in the phase separation of the polymer. A decrease in the carbonyl ratio, however, may result from the urethane N–H hydrogen bonding with either the polyether oxygen or the urethane alkoxy oxygen.

As shown in Table II for the mixed polyol samples, incorporation of 5–14 wt % FPEG had no significant effect on the polymers' hydrogen bonding characteristics. The ratio of bonded–free carbonyl was essentially the same for all the mixed soft segment polymers, indicating similar degrees of phase mixing.

For the pure FPEG soft segment polymers, the hard segment content had no significant effect on the hydrogen bonding characteristics of the polymers. The bonded carbonyl absorbance band for the MDEA-chain-extended polymer M34-F66 shifted to a higher frequency 1712 cm^{-1}, indicating a change in the environment of the bonded carbonyl. Ionization significantly decreased the bonded–free carbonyl ratio probably due to the hydrogen bonding of the urethane N–H groups with the polar sulfonate groups.

A distinct S–O absorbance peak at 1040 cm^{-1} due to the sulfonate group was observed for M34-F66-S8.

Thermal Analysis

Figure 3 contains representative DSC curves for the first heating of the FPEG-based, PTMO-based, and the copolymerized mixed polyol soft segment polymers, B50-F50, B48-F0, and B45-F14 respectively. The thermal transition results are summarized in Table III. All the polymers have a glass transition temperature (T_g) and two endotherms attributed to the disruption of short- and long-range order of the hard segment domains.

The glass transition temperatures for the soft segment constituents, as pure homopolymers, are −85°C for PTMO[26] and −59°C for FPEG, as determined using DSC. The thermal transitions of block copolymers are altered from the homopolymer transition temperatures due to mobility restrictions resulting from covalent bonding of the hard and soft segments.[27] Phase mixing of the high T_g hard segment phase with the soft segment phase also increases the T_g of a polymer.[3,27]

As indicated in Table III, the incorporation of a low weight percentage of FPEG (5–14 %) into the polymer backbone has essentially no effect on the soft segment T_g. Blends of the FPEG and PTMO polyols, ranging from 5 to 14 wt % FPEG, were opaque indicating that the polyols were immiscible. The DSC results for the blended polyols showed that the addition of FPEG did not

TABLE II
Infrared Spectroscopy Results

Material	Bonded/free C=O (A_{1700}/A_{1730})
B48-F0	1.5
B47-F5	1.4
B46-F9	1.1
B45-F14	1.4
B43-F9-EO8	1.2
B50-F50	1.2
B33-F67	1.1
M34-F66	0.9
M34-F66-S8	0.3

inhibit the crystallization of the PTMO polyol even at quench rates of 320°C/min. From these results it is hypothesized that the polymer morphology consists of three phases primarily composed of PTMO, FPEG, and the hard segment phase. A T_g for FPEG-rich phase is not detectable using DSC due to the low percentage of FPEG incorporated. Similar results were found for polydimethylsiloxane (PDMS) and PTMO mixed soft segment polymers.[28]

As shown in Figure 3, the short-range order endotherm shifted to higher temperatures and began to merge with the long-range order endotherm. The short-range order endotherm is primarily dependent on the polymer's thermal history. The shift in the endotherm to higher temperature is due to sample storage and drying procedures prior to testing. The long-range order endotherm reflects the interaction between the soft and hard segment. The long-range order endotherms were broader for the mixed soft segment polymers relative to B48-F0. This broadening effect was most dramatic for the THF/EO soft segment polymer. The greater polarity of the THF/EO soft segment may promote phase mixing of the hard segment.

The relatively high T_gs for the pure FPEG soft segment polymers compared with the T_g of the FPEG polyol indicates there is some hard segment dispersed in the soft segment phase. The relatively polar polyether backbone of the FPEG polyol would be expected to be more compatible with the hard segment phase than the nonpolar fluorine-containing pendant group. The fluorine-containing pendant chain should orient away from the hard segment. The higher T_g of B50-F50 compared with B33-F67 is attributed to the greater number of single MDI unit hard segments in B50-F50 that are more soluble in the soft segment phase.[27] The enhanced interaction between the soft segment phase and the hard segment phase of B50-F50 is verified by its lower hard segment dissociation temperature.

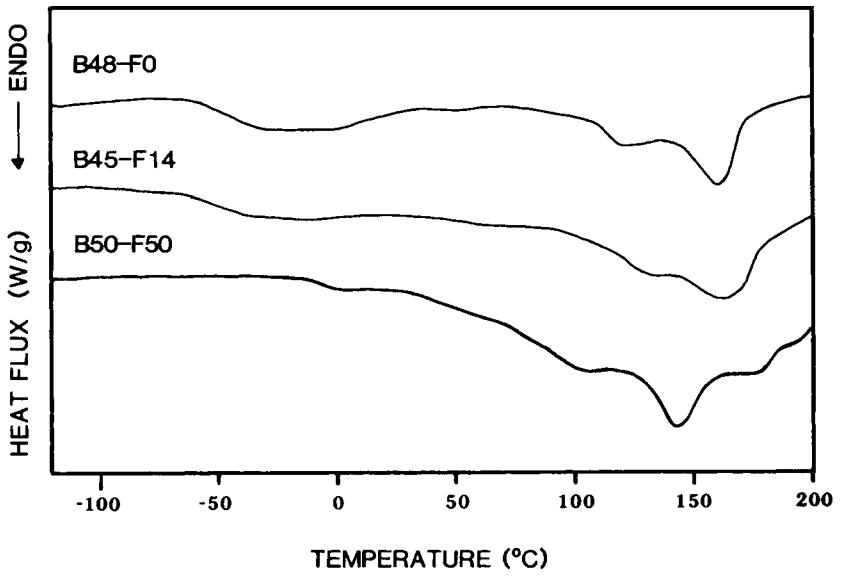

Fig. 3. DSC curves for B50-F50, B48-F0, and B45-F14.

TABLE III
Transition Data

Material	Differential scanning calorimetry			Dynamic mechanical properties	
	T_g Midpoint (°C)	Glass transition range (°C)	High-temperature endotherm (°C)	γ Peak (°C)	T_g (°C)
B48-F0	−49	47	162	−131	−32
B47-F5	−48	51	162	−128	−35
B46-F9	−48	40	153	−128	−31
B45-F14	−50	31	164	−128	−32
B43-F9-EO8	−48	48	148	−128	−30
B50-F50	−10	13	142	−133	10
B33-F67	−17	38	160	−130	−14
M34-F66	−12	25	166	−130	−2
M34-F66-S8	−22	46	—	−132	−8
PFEG (1899 MW)	−59	11			

The higher T_g and absence of a high-temperature endotherm for the MDEA-chain-extended polymer, M34-F66, indicated it was more phase mixed than its BD-extended analog. The methyl pendant group of the MDEA disrupts the hard segment packing, thereby enhancing phase mixing.[29,30] Ionization of the MDEA-chain-extended polymer increased the degree of phase separation as indicated by the dramatic decrease in the soft segment phase T_g and the appearance of a short-range order endotherm at 117°C. The propyl sulfonate groups increase the polarity difference between the segments, thereby enhancing phase separation. These results are in agreement with previous studies investigating MDEA-chain-extended polyurethane ionomers.[31]

Dynamic Mechanical Analysis

The dynamic mechanical analysis (DMA) results for the polymers are presented in Figures 4 and 5 and the transition data are summarized in Table III. The low-temperature transition (γ peak) and the glass transition temperature of the soft segment (α peak) are determined from the peak positions in the loss modulus (E'') curve. In general the transition temperatures determined by DMA are higher than the values determined by DSC, due to the difference in the time scale of the experiments.[3,32,33] The low-temperature transition (γ peak) is attributed to the local mode motion of primarily PTMO in the mixed soft segment polymers and the BD segments for the 100% FPEG soft segment polymers.[3]

The DMA curves for B48-F0, B45-F14, and B43-F9-E08 shown in Figure 4 are similar to the curves for B47-F5 and B46-F9 (not shown). There is no significant difference in the T_gs of the mixed soft segment polymers. The rubbery plateau modulus, however, was slightly reduced with increasing FPEG incorporation.

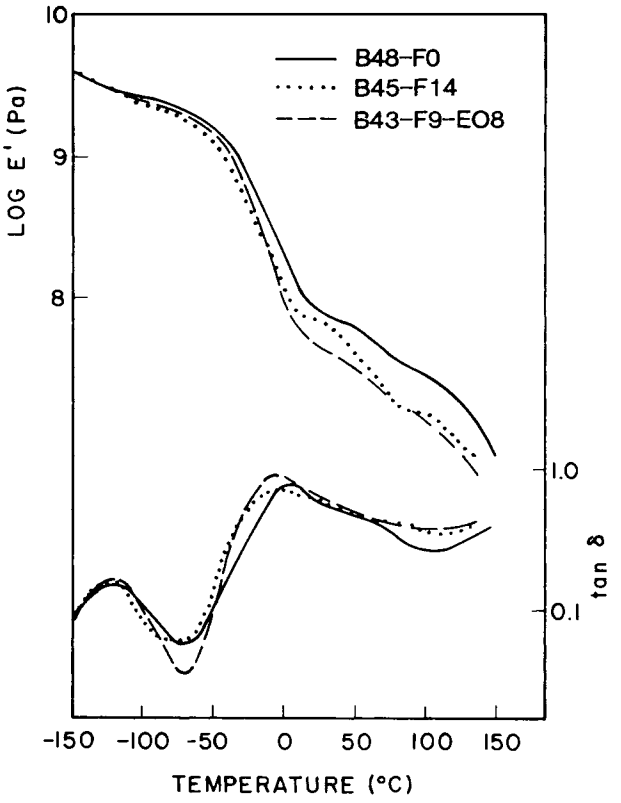

Fig. 4. Dynamic mechanical spectra of the copolymerized mixed soft segment polymers.

The DMA curves for the 100% FPEG polymers in Figure 5 show that B50-F50 has a higher T_g, broader α peak, and a higher rubbery plateau modulus than B33-F67. These enhanced properties are attributed to the increased size and interconnectivity of the hard segment domains. The MDEA-extended polymer was more phase mixed than its BD-extended analog as indicated by its higher T_g. Ionization of the MDEA-chain-extended polymer improved the domain cohesion and phase separation of the polymer resulting in an enhanced plateau modulus that extended to higher temperatures.

Tensile Properties

The stress–strain curves for the mixed soft segment polyurethanes and the pure FPEG soft segment polyurethanes are shown in Figures 6 and 7, respectively. The strength and elastic properties of the polyurethanes are listed in Table IV.

For the mixed soft segment polyurethanes, as the FPEG content increases the mechanical properties decrease, as shown in Figure 6. The stress–strain behavior of B45-F14 (not shown) is similar to B46-F9. The decrease in mechanical strength, modulus, and elongation is attributed to the bulky fluorinated side group of FPEG, which prevents crystallization of the soft segment upon extension and increases interchain separation.[34] This is evidenced by the absence

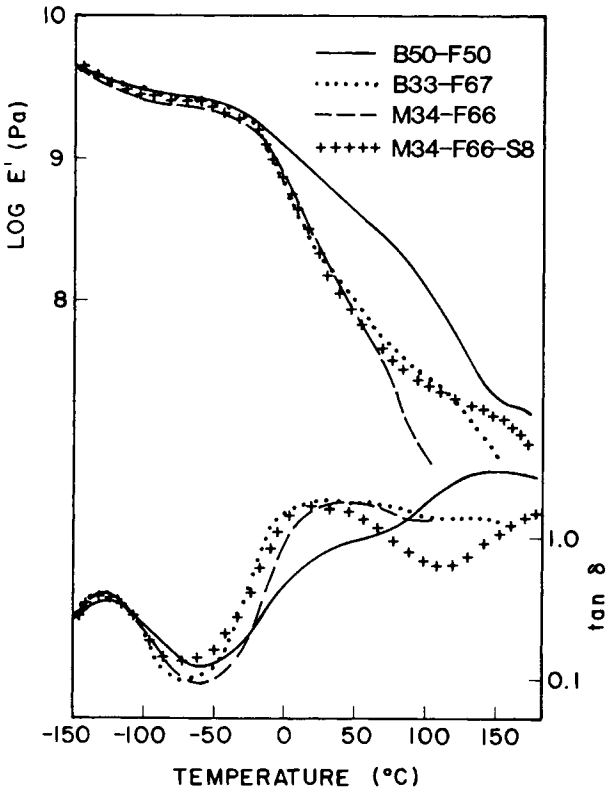

Fig. 5. Dynamic mechanical spectra of the 100% FPEG soft segment polymers.

of strain hardening in the stress–strain curves. The decrease in Young's modulus and 100% tensile modulus with FPEG content is in agreement with the lowered DMA rubbery plateau modulus discussed in the previous section. The incorporation of EO into the soft segment of B43-F9-EO8 dramatically decreased the ultimate strength and elongation of the polymer while increasing the Young's modulus.

For the pure FPEG soft segment polymers, the ultimate strength and Young's modulus are highest for B50-F50, which exhibited the stress–strain behavior of a tough plastic. B50-F50's higher strength and moduli are attributed to an increase in the hard segment content and block length, along with a more interconnected hard segment domain morphology.[27,35] The lower tensile strength and modulus for the MDEA-extended polymers is due to the inability of the MDEA-based hard segments to crystallize. Upon ionization the enhancement of the polarity difference between the segments promoted phase separation thereby increasing the strength and modulus of the polymer. These results indicated that hard-domain cohesiveness is a major factor determining the tensile properties of these 100% FPEG soft segment polyurethanes.

Surface Analysis

X-ray photoelectron spectroscopy (XPS) was used to investigate the composition and chemistry of the air-cast surfaces of each polymer. The elemental

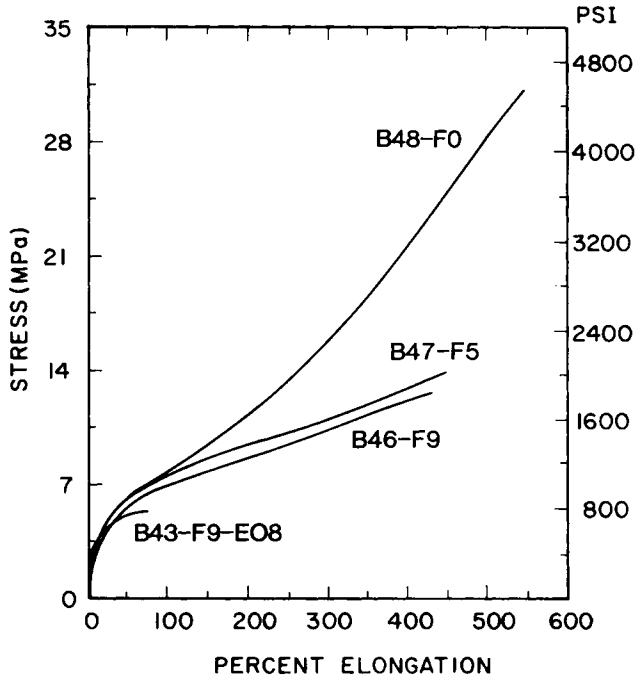

Fig. 6. Stress–strain curves for the copolymerized mixed soft segment polymers.

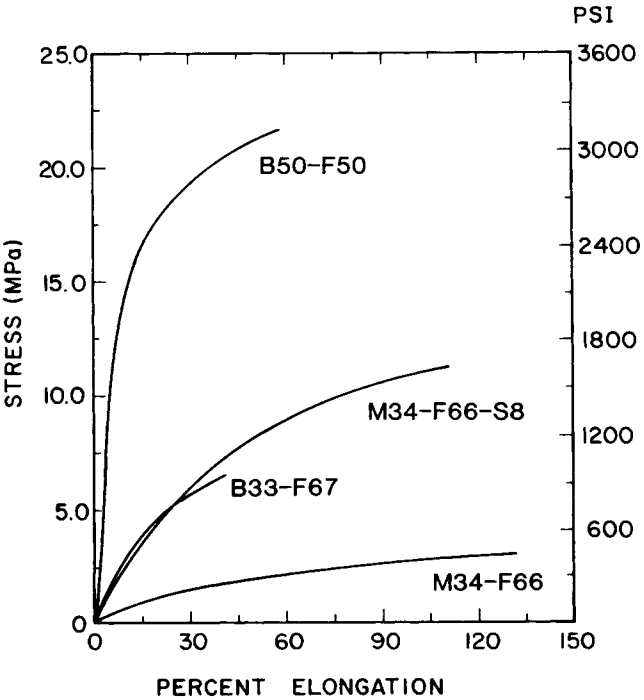

Fig. 7. Stress–strain curves for the 100% FPEG soft segment polymers.

TABLE IV
Mechanical Properties

Material	Young's modulus (MPa)	100% secant modulus (MPa)	Ultimate stress (MPa)	Percent elongation at break
B48-F0	37.1	7.5	31.6	560
B47-F5	30.3	6.8	13.8	450
B46-F9	30.0	6.3	12.9	440
B45-F14	25.5	4.9	12.5	430
B43-F9-EO8	40.6	—	5.4	80
B50-F50	184.7	—	21.6	60
B33-F67	28.9	—	6.6	40
M34-F66	9.1	2.0	3.1	130
M34-F66-S8	26.1	10.2	11.3	110

atomic percentages listed in Table V were calculated from the bulk polymer stoichiometries and determined from the XPS analysis performed at a take-off angle of 45°.

The fluorine and the fluorocarbon, CF_2 and CF_3, photoemission peaks are representative of the soft segment phase while the nitrogen and carbonyl peaks are representative of the hard segment phase. The trends in the atomic percentages of these peaks, therefore, can be correlated with the polymer's surface morphology. Fluorine has a high photoemission cross section and high electronegativity that enhances its detectability. The intensity of the N_{1s} signal is relatively weak.

Fluorine-containing molecules generally have very low surface energies, thus it is expected that the FPEG segment of the polyurethane will orient at the air interface to minimize the interfacial energy. As indicated in Table V, the fluorine concentration for all of the mixed polyol polyurethanes is much greater than the bulk concentration indicating that as expected the FPEG soft segment is enriched at the surface. A measure of the level of surface enhancement of the FPEG macroglycol is given by the difference between the experimental and bulk fluorine concentrations. This quantity is referred to as ΔF. The surface

TABLE V
ESCA Analysis (Atomic Percent)

	F		ΔF	CF_2		CF_3		N		C=O		Si
Material	Bulk	Exp	Bulk − Exp	Bulk	Exp	Bulk	Exp	Bulk	Exp	Bulk	Exp	Exp
B48-F0	—	—	—	—	—	—	—	4.4	3.2	4.4	3.8	1.5
B47-F5	2	26	24	0.6	5.9	0.1	1.7	4.4	2.6	4.4	1.9	0.0
B46-F9	3	30	27	1.3	9.0	0.3	1.8	4.3	1.6	4.3	1.0	0.0
B45-F14	5	35	30	1.9	8.0	0.4	2.1	4.2	1.9	4.2	1.2	0.1
B43-F9-EO8	3	33	30	1.2	7.4	0.3	2.0	4.0	2.2	4.0	2.4	0.0
B50-F50	18	34	16	7.0	9.7	1.5	4.6	4.6	3.0	4.7	3.2	0.1
B33-F67	25	36	11	9.5	9.7	2.1	2.3	3.2	2.4	3.2	2.2	0.1
M34-F66	25	34	9	9.4	9.1	2.1	2.1	4.2	3.2	3.2	2.2	0.1
M34-F66-S8	23	29	6	8.7	8.2	1.9	2.1	3.9	3.6	2.9	2.8	0.1

enrichment of FPEG increased with increasing FPEG content for the mixed soft segment polymers. The higher ΔF for B43-F9-E08 compared with B46-F9 is attributed to the greater polarity of the THF/EO macroglycol, which promotes this segregation.

The experimentally determined atomic fluorine concentration is greater than the fluorine content calculated from the sum of the C–F groups ($2CF_2 + 3CF_3$). This discrepancy may be due to a preferential orientation of the fluorine atoms at the surface relative to the carbon atoms. The photoelectron intensity decreases as the sample depth the photoelectron originates from increases. The following equation describes the intensity attenuation:

$$I(x) = I_0(x)\exp(-x/\lambda)$$

where $I_0(x)$ is the intensity from photoelectrons originating at a depth x below the surface, $I(x)$ is the intensity that is measured at the surface, and λ is the inelastic mean free path of an electron having a particular kinetic energy.[36] Thus a surface layer of fluorine atoms would have a greater $I(x)$ than the deeper carbon atoms.

The nitrogen and carbonyl concentrations for the mixed polyol polymers are significantly depleted at the surface relative to the bulk. The increased polarity of the THF/EO soft segment enhanced the amount of hard segment at the surface relative to B46-F9 suggesting that it is more polar than either the FPEG or the hard segment phases.

The surfaces of all the 100% FPEG soft segment polymers were enriched with the FPEG macroglycol segment. Surface enrichment of fluorine was lower for the more phase mixed morphology of the MDEA-based polyurethanes compared with the BD-extended polymers. Sulfur was detected on the surface of M34-F66-S8 (0.9 atom%). The low ΔF and relatively high C=O and N concentrations indicate that the M34-F66-S8 surface is phase mixed.

Silicon contamination, probably in the form of siloxane, was found on all the polyurethanes studied.

Contact Angle

Underwater contact angle results, using air and octane as probe fluids, provide information about the hydrated surface morphology of the polymers. The average surface–water–air and surface–water–octane contact angles are listed in Table VI.

As expected the incorporation of FPEG into the PTMO-based polyurethanes increased the hydrophobicity of the polymer surface. The hydrophobic character of the surface appeared to plateau for FPEG concentrations of $\geq$ 9 wt % as indicated by the contact angles for B46-F9 and B45-F14. Similar results were observed by Ito and co-workers[37] for polyurethanes containing greater than 7 wt % of a fluorinated diol chain extender or a fluorinated polyether. The enhanced polarity of the THF/EO macroglycol segment increased the polarity of B43-F9-E08's surface compared with B46-F9.

The air and octane underwater contact angles for B33-F67 and B50-F50 are approximately equal despite B50-F50's greater hard segment content. The discrepancies in the air and octane contact angles of B50-F50 and B33-F67 com-

TABLE VI
Static Contact Angle Data[a]

Material	Surface–water–air contact angle ± SD	Surface–water–octane contact angle ± SD
B48-F0	59 ± 5	84 ± 4
B47-F5	53 ± 3	98 ± 6
B46-F9	72 ± 3	134 ± 5
B45-F14	72 ± 3	130 ± 4
B43-F9-EO8	68 ± 5	103 ± 4
B50-F50	79 ± 3	111 ± 5
B33-F67	75 ± 4	106 ± 4
M34-F66	56 ± 2	92 ± 4
M34-F66-S8	38 ± 5	54 ± 6

[a] 48 h at 25°C

pared with B46-F9 and B45-F14 suggests that the effect of FPEG on the polarity of the polymer surface may be complicated by the complex structure of the FPEG macroglycol.

M34-F66 is significantly more hydrophilic than its BD-extended analog due to the added polarity of the tertiary nitrogen in the MDEA chain extender. As expected, the incorporation of sulfonate groups significantly enhanced the polarity of M34-F66-S8's surface.

Dynamic Contact Angle

Dynamic contact angle measurements provide information about the time dependence of the contact angle and the dynamic nature of the surface upon exposure to water. The air-equilibrated polymer film that initially comes in contact with water is enriched in the relatively nonpolar soft segment. The advancing contact angle θ_A is characteristic of the repulsion of water from this hydrophobic surface. As the film is wetted, the surface will rearrange to reduce the interfacial free energy by orienting the more polar components at the surface.

TABLE VII
Dynamic Contact Angle Results

	θ_A		θ_R		$\theta_A - \theta_R$	
Material	Cycle 1	Cycle 2	Cycle 1	Cycle 2	Cycle 1	Cycle 2
B48-F0	80 ± 1	80 ± 1	49 ± 1	48 ± 2	31	32
B47-F5	97 ± 5	94 ± 2	65 ± 5	66 ± 6	32	28
B46-F9	95 ± 3	91 ± 2	62 ± 6	63 ± 7	33	28
B45-F14	102 ± 3	98 ± 4	62 ± 3	62 ± 4	40	36
B43-F9-EO8	98 ± 2	95 ± 1	63 ± 1	64 ± 2	35	31
B50-F50	121 ± 2	120 ± 2	63 ± 6	63 ± 5	58	57
B33-F67	123 ± 2	117 ± 2	34 ± 9	31 ± 8	89	86
M34-F66	122 ± 2	122 ± 3	8 ± 8	4 ± 8	114	118
M34-F66-S8	119 ± 2	120 ± 1	0 ± 0	0 ± 0	119	120

The lower receding angle θ_R is characteristic of the rearranged hydrophilic surface at the water–polymer interface. The difference between the advancing and receding angles is the contact angle hysteresis, which is a measure of the wettability, heterogeneity, mobility, roughness, and deformation of the surface.[22]

The advancing and receding contact angles shown in Table VII are the average from a minimum of three coated slides. For the mixed polyol polyurethanes the presence of FPEG increased the nonpolar character of the air-equilibrated surface, as indicated by the high advancing angles. This is in agreement with the XPS results that indicated the surface was enriched in FPEG. The advancing angles appeared to be independent of the FPEG content. The higher θ_As for the pure FPEG soft segment polymers indicated that the mixed soft segment surfaces must contain a mixture of both PTMO and FPEG domains.

The receding angles for the mixed soft segment polymers were higher for the FPEG-containing polymers compared to B48-F0. Thus the surface rearranged to lower its interfacial energy by exposing more hard segment at the surface but some FPEG and PTMO domains must also be present at the surface to account for the higher receding angles. The degree of phase mixing at the surface was independent of the FPEG content. The THF/EO soft segment had no significant effect on either θ_A or θ_R.

The advancing contact angles for the pure FPEG-containing polymers are dependent on the presence of FPEG, but independent of its concentration. The receding contact angles are dependent on the polarity and content of the hard segment phase. B50-F50's θ_R is similar to the mixed soft segment polymers indicating it has a phase mixed surface morphology that may result from its relatively phase mixed bulk morphology. B33-F67 rearranged to orient a greater amount of the polar hard segment at the surface as indicated by its much lower θ_R. The greater polarity difference between FPEG and the hard segment for B33-F67, compared with PTMO and the hard segment for B48-F0, enhanced the preferential segregation of the hard segment at the surface as indicated by its large hysteresis.

The MDEA-chain-extended polymer is considerably more polar than its BD analog due to the increased polarity of the tertiary amine in the MDEA. As expected sulfonation further increased the polarity of the surface resulting in completely wettable surface.

The angles for the second cycle indicated that in the short time period of this test, approximately 4 min, the polymer surfaces repeatedly rearranged to lower their interfacial energy. These results indicate that at least for the first two cycles the contact angles are kinetically limited.

CONCLUSIONS

A novel series of poly(fluoralkylether)urethanes, which possess interesting bulk and surface properties, has been synthesized. The incorporation of the fluoropolyether macroglycol into the polyurethane structure was verified by the presence of two C–F absorbance peaks observed in the polymers' IR spectra.

The bulk property results indicated that the incorporation of 5, 9, or 14 wt % FPEG had essentially no effect on the glass transition of the polymers and their phase separation. Blends of the PTMO and FPEG polyols are immiscible,

thus it is hypothesized that there are three phases present in these copolymerized mixed soft segment polymers. The tensile strength and Young's modulus of the copolymerized mixed macroglycol polyurethanes were slightly reduced by increasing FPEG content while the elongation remained unaffected.

The incorporation of FPEG, even as low as 5 wt %, resulted in dramatically increasing the surface fluorine concentration, as determined using XPS. The dynamic contact angles, θ_A and θ_R, for the mixed soft segment surfaces indicated the surfaces were phase mixed. The degree of phase mixing was independent of the FPEG content. For the polymer surface equilibrated in water, the hydrophobicity of the polymer surface reached a maximum at a FPEG content of 9 wt %, as indicated by the static contact angle results.

The morphology and mechanical properties of the pure FPEG soft segment polymers are strongly dependent on the percentage of hard segment and the type of chain extender used. The BD-chain-extended polymer was more phase separated than its MDEA-extended analog. Propyl sulfonate incorporation onto the MDEA-chain-extended polymer backbone enhanced phase separation. The highest hard segment containing polymer, B50-F50, exhibited the stress–strain behavior of a tough plastic, while the other polymers showed typical elastomeric behavior. The tensile properties were lower for the more phase mixed MDEA-chain-extended polymer.

The surfaces of the pure FPEG soft segment polymers were enriched in the FPEG soft segment. The morphology of the polymer surface, as indicated by XPS and contact angle measurements appeared to be controlled by the polymers' bulk morphology and the polarity of the testing environment.

The results presented here show that fluorinated polyurethanes can be readily synthesized to have mechanical properties ranging from a tough plastic to an elastomer, while having a low surface energy, fluorine-enriched surface in both air and water environments. These fluorinated polymers would be useful for applications requiring both the elastomeric properties of a polyurethane and low surface friction.

The authors acknowledge Robert Schumacher for his assistance in obtaining the bulk property data. The work was supported by NIH Grants HL-21001 and HL-24046 and the Office of Naval Research.

References

1. G. M. Estes, S. L. Cooper, and A. V. Tobolsky, *J. Macromol. Sci. Rev. Macromol. Chem.*, **4**, 313 (1970).

2. A. Noshay and J. E. McGrath, *Block Copolymers: Overview and Critical Survey*, Academic Press, New York, 1977.

3. P. E. Gibson, M. A. Vallance, and S. L. Cooper, in *Developments in Block Copolymers, I.* I. Goodman, Ed. Applied Science Publishers, New York, 1982, pp. 217–259.

4. F. Gosnell and J. Hollander, *J. Macromol. Sci. Phys.*, **B1**(4), 831 (1967).

5. E. G. Shafrin and W. A. Zisman, *J. Phys. Chem.*, **64**, 519 (1960).

6. J. R. Griffith and J. D. Bultman, *Ind. Eng. Chem. Prod. Res. Dev.*, **17**, 8 (1978).

7. E. P. Wesseler, R. Iltis, and L. C. Clark, Jr., *J. Fluorine Chem.*, **9**, 137 (1977).

8. D. L. Hunston, J. R. Griffith, and R. C. Bowers, *Ind. Eng. Chem. Prod. Res. Dev.*, **17**, 8 (1978).

9. J. G. Reiss and M. Le Blanc, *Angew: Chem. Int. Ed. Engl.*, **17**, 621 (1978).

10. J. Hollander, F. D. Trischler, and E. S. Harrison, *Polym. Prepr. Am. Chem. Soc. Div. Polym. Chem.*, **8**, 1149 (1967).

11. T. M. Keller, *J. Polym. Sci. Polym. Chem. Ed.*, **23,** 2557 (1985).
12. J. Hollander, F. D. Trischler, and R. B. Gosnell, *J. Polym. Sci. Part A-1,* **5,** 2757 (1967).
13. S. C. Yoon and B. D. Ratner, *Macromolecules,* **19,** 1068 (1986).
14. M. D. Lelah, T. G. Grasel, J. A. Pierce, and S. L. Cooper, *J. Biomed. Mater. Res.*, **19,** 1011 (1985).
15. J. H. Scofield, *J. Electron. Spectrosc. Relat. Phenom.*, **8,** 129 (1976).
16. A. Proctor and D. M. Hercules, *Appl. Spectrosc.*, **38**(4), 505 (1984).
17. P. A. Jansson, *Deconvolution with Applications in Spectroscopy,* Academic Press, Orlando, Florida, 1984.
18. H. R. Thomas and J. J. O'Malley, *Macromolecules,* **12,** 323 (1979).
19. D. T. Clark, W. J. Feast, D. Kilcast, and W. K. R. Musgrave, *J. Polym. Sci. Polym. Chem. Ed.*, **11,** 389 (1973).
20. A. Takahara, N. Higashi, T. Kunitake, and T. Kajiyama, *Macromolecules* **21,** 2443 (1988).
21. W. C. Hamilton, *J. Colloid Interface Sci.*, **40,** 219 (1972).
22. J. D. Andrade, L. M. Smith, and D. E. Gregonis, in *Surface and Interfacial Aspects of Biomedical Polymers, I., Surface Chemistry and Physics,* J. D. Andrade, Ed., Plenum Press, New York, 1985, pp. 249–292.
23. J. Brandrup and E. H. Immergut, Eds., *Polymer Handbook,* Wiley, New York, 1975.
24. K. Knutson and D. J. Lyman, *Biomaterials: Interfacial Phenomena and Applications,* S. L. Cooper and N. A. Peppas, Eds., Advances in Chemistry Series, **199,** 109–132 (1982).
25. J. C. West and S. L. Cooper, *J. Polym. Sci. Polym. Symp.*, **60,** 127–150 (1977).
26. J. A. Faucher and J. V. Koleske, *Polymer,* **9,** 44 (1968).
27. J. A. Miller, S. B. Lin, K. K. S. Hwang, K. S. Wu, P. E. Gibson, and S. L. Cooper, *Macromolecules,* **18,** 32 (1985).
28. R. A. Phillips, J. Castles Stevenson, M. R. Nagarajan, and S. L. Cooper, *J. Macromol. Sci. Phys.*, **B27,** 245–274 (1988).
29. T. A. Speckhard, K. K. S. Hwang, C. Z. Yang, W. R. Laupan, and S. L. Cooper, *Macromolecules,* **B23**(2), 175 (1984).
30. K. K. S. Hwang, C. Z. Yang, and S. L. Cooper, *Polym. Eng. Sci.*, **21,** 1027 (1981).
31. J. A. Miller, K. K. S. Hwang, and S. L. Cooper, *J. Macromol. Sci. Phys.*, **B22**(2), 321–341 (1983).
32. J. D. Ferry, *Viscoelastic Properties of Polymers,* Wiley, New York, 1980, p. 280.
33. J. J. Alkonis and W. J. MacKnight, *Introduction to Polymer Viscoelasticity,* Wiley, New York, 1983, p. 57.
34. T. A. Speckhard and S. L. Cooper, *Rubber Chem. Tech.*, **59,** 405 (1985).
35. C. Hepburn, *Polyurethane Elastomers,* Applied Science Publishers, London, 1982.
36. A. F. Orchard, in *Handbook of X-ray and Ultraviolet Photoelectron Spectroscopy,* D. Briggs, Ed., Heydon, London, 1977, pp. 1–15.
37. Y. Ito, T. Kashiwagi, S. Q. Liu, L. S. Liu, Y. Kawamura, Y. Iguchi, and Y. Imanishi, in *Proceedings of the 2nd International Symposium on Artificial Heart and Assist Device,* Tokyo, Japan, Aug. 1987, Springer-Verlag, Tokyo, 1988.

Received July 24, 1989
Accepted November 20, 1989